Hindawi
Journal of Sensors
Volume 2018, Article ID 2740679, 12 pages
https://doi.org/10.1155/2018/2740679

Research Article

Online Accurate Estimation of the Wheel-Rail Adhesion Coefficient and Optimal Adhesion Antiskid Control of Heavy-Haul Electric Locomotives Based on Asymmetric Barrier Lyapunov Function

Kaihui Zhao, Peng Li, Changfan Zhang, Jing He, Yanfei Li, and Tonghuan Yin

College of Electrical and Information Engineering, Hunan University of Technology, Zhuzhou 412007, China

Correspondence should be addressed to Changfan Zhang; zhangchangfan@263.net

Received 18 October 2017; Accepted 17 January 2018; Published 8 April 2018

Academic Editor: Jesus Corres

This paper proposes a new scheme of online accurate estimation of wheel-rail adhesion coefficient and optimal adhesion antiskid control of heavy-haul electric locomotives (HHEL) based on sliding mode and asymmetric barrier Lyapunov function (ABLF) theory. To achieve optimal adhesion control of the HHEL, it is necessary to precisely estimate the wheel-rail adhesion coefficient. However, the adhesion coefficient is difficult to be measured with a conventional physical sensor. The first novelty of this paper is to design a smart adhesion coefficient sensor based on sliding mode observer (SMO). The perception of the adhesion coefficient is transformed into the observation of load torque of the traction motors, and the wheel-rail adhesion coefficient is further calculated by using the load torque observed value. The HHEL achieves maximum traction from operating in the optimal adhesion point. However, wheel skidding is most likely to occur at this point. According to the changing trend of the adhesive coefficient characteristic curve, the operating state of a locomotive can be divided into two regions: the stable and skid regions. The second novelty of this paper is the adaptation of ABLF to guarantee that the HHEL operated at a stable region and the optimal adhesion antiskid control of HHEL is achieved. Finally, the simulation and experimental results verify the feasibility and effectiveness of the proposed method.

1. Introduction

Heavy-haul electric locomotives (HHEL) that are widely used in railway freight are characterized by high tractive forces. However, the effective use of traction power of the HHEL is limited by the wheel-rail adhesion conditions, which is affected by temperature, humidity, and surface condition. To achieve the optimal adhesion control required for the HHEL, it is necessary to precisely estimate the wheel-rail adhesion coefficient. But the adhesion coefficient is difficult to be measured with a conventional physical sensor [1]. Advanced sensor is one of the essential components of the HHEL control system. The high-precision sensor can accurately monitor, quickly feedback, and be insensitive to external disturbances, which effectively improves the performance of the control system [2]. Therefore, an advanced adhesion coefficient sensor is necessary to enable the HHEL to achieve optimal adhesion control and exert maximize traction.

Recent studies have focused on obtaining the adhesion coefficient of the locomotive. The method of full-state observer is presented to observe the adhesion coefficient for subway trains in [3]. However, the feedback gain matrix has a large effect on the accuracy of the observer. The Kalman filter method is used to estimate the locomotive adhesion coefficient in [4], which requires a larger data capacity.

In practice, the observation of the adhesion coefficient can be converted into the estimate of the traction motor load torque; then, the adhesion coefficient can be calculated by the observed value of the load torque. Sliding mode control method has good robustness to parameter variations and external disturbance [5]. The method of observing the permanent magnet synchronous motor

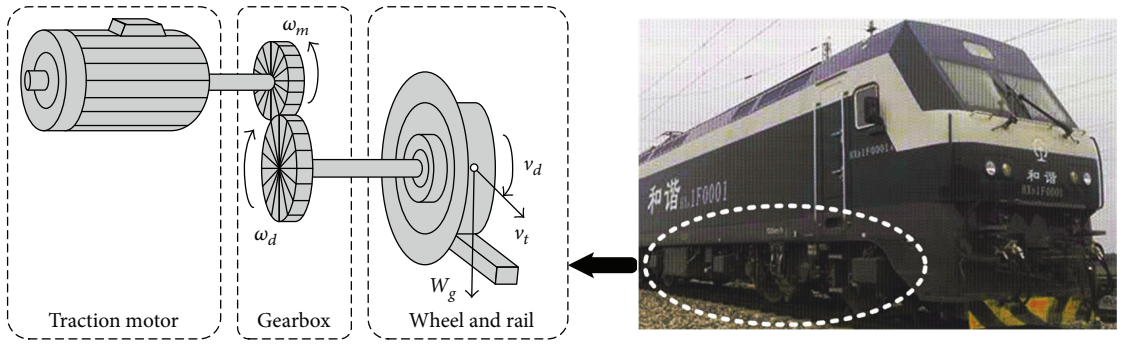

Figure 1: Simplified wheel-rail model of the HHEL.

(PMSM) load torque is proposed by the sliding mode observer in [6], which obtains better observation accuracy. A cascade sliding mode observer is designed to observe the derivative of the adhesion coefficient, and a better control effect is achieved in [7].

In order to effectively utilize locomotive traction power, a considerable number of researchers have focused on obtaining optimal adhesion control [8, 9]. However, according to the changing trend of the adhesive coefficient characteristic curve, the creep velocity of locomotives must be constrained at the stable region to avoid wheel skidding. Traditional readhesion control is obtained through detecting the wheel slip rapidly and adjusting torque to make the locomotive return to the stable region. The disadvantage of this traditional approach is that it cannot completely eliminate the skidding phenomenon [10].

In recent years, the barrier Lyapunov function (BLF) state-constrained control method has been paid attention by scholars. The BLF technology is also applied to the stable control of high-speed trains, and the creep state is limited in the stable area, which ensures the safety of train operation and the comfort of passengers [11, 12]. Because the barrier boundaries of the BLF control technique are symmetric, the obstacle region inevitably includes the skid region. Therefore, the stability of control cannot be guaranteed [13]. The ABLF theory is presented in [14], in which barrier boundaries can be designed according to the requirements of different constraints; the initial conditions of the ABLF can be more relaxed than those of the BLF. The work in [15] proposes a brake control system for aircraft landing using the ABLF to avoid aircraft locking during braking.

Inspired by the above surveys, the adhesion coefficients of HHEL are estimated accurately in real time by using the sliding mode control method [6, 7], and the optimal antiskid wheel control method for the HHEL is proposed based on the ABLF algorithm [14, 15] to operate locomotives in the stable region while near the optimal adhesion point. The proposed method ensures optimal adhesion control and antiskid control and effectively utilizes the HHEL traction power.

The rest of this paper is organized as follows. In Section 2, the model of the wheel-rail system of the HHEL is described. In Section 3, a sliding mode observer is designed to observe the adhesion coefficient. In Section 4, an ABLF controller is designed, and its stability is analyzed. In Section 5, simulations and experiments are conducted to verify the effectiveness of the proposed method. In Section 6, conclusions are presented.

2. Description of the Wheel-Rail System of the HHEL

The simplified wheel-rail model of a locomotive is shown in Figure 1. The model is composed of three parts, traction motors, gear box, and wheel and rail [16]. The traction equipment's main task is to transmit the traction torque of the traction motors to the wheelsets of the locomotive through the gearboxes and drive the wheel such that it rotates at a speed of v_d. During the traction operation process, wheel speed v_d is always greater than vehicle speed v_t. Generally, creep speed v_s can be defined as the speed difference between the wheel speed and the vehicle speed. The locomotive is driven to move forward by the adhesion force F_μ from the creep phenomenon between the wheel and the rail.

2.1. Dynamic Model of the Locomotive Wheel. With the damping coefficient ignored, the traction motor equation is as follows [16]:

$$\begin{aligned} J_m \frac{d\omega_m}{dt} &= T_m - T_L, \\ T_L R_g &= F_\mu r, \end{aligned} \tag{1}$$

where T_m is the electromagnetic torque of the traction motor $(\mathrm{N}\cdot\mathrm{m})$, T_L is the load torque $(\mathrm{N}\cdot\mathrm{m})$, ω_m is the rotor angular velocity (rad/s), r is the radius of the wheel (m), J_m is the moment of inertia of the traction motor $(\mathrm{kg}\cdot\mathrm{m}^2)$, F_μ is the adhesion force between the wheel and the rail (N), and R_g is the speed ratio of the gear box, which is written as follows:

$$Rg = \frac{\omega_m}{\omega_d}, \tag{2}$$

where ω_d is the angular velocity of the wheel (rad/s).

Substituting (2) into (1), the dynamic model of the locomotive wheel is

$$J_m \frac{R_g^2}{r^2} \frac{dv_d}{dt} = \frac{R_g}{r} T_m - F_\mu. \tag{3}$$

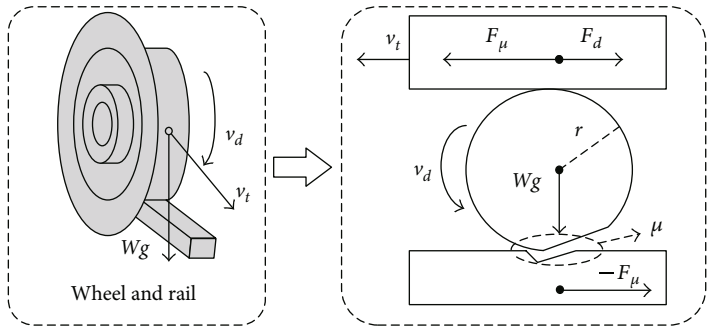

Figure 2: Schematic of the wheel rail adhesion.

2.2. Dynamic Model of the Full Locomotive. The mechanical dynamics of the HHEL with 8 axles is defined as follows [17]:

$$M\frac{dv_t}{dt} = \sum_{i=1}^{8} F_{\mu i} - F_d,$$
$$F_d = \left(l + pv_t + qv_t^2\right)Mg, \tag{4}$$

where M is the total quality of both the locomotive and load (kg); $F_{\mu i}$ is the adhesion force for the traction motor of the i axle (N); F_d is the sum of retardation forces (N), which is closely related to vehicle speed v_t; and l, p, and q are retardation coefficients, all of which are positive constants.

2.3. Adhesion Characteristic Curve of the Wheel and Rail. The adhesion coefficient μ is used to characterize the complex mechanical relationship between the wheel and the rail. The schematic of the mechanism of wheel-rail adhesion is shown in Figure 2. The microdeformation region occurs in the wheel-rail contact region when the wheels rotate as the result of the action of the axle load W. Then, the adhesion force F_μ is produced by the interaction between the wheel and the rail.

The adhesion force F_μ and the adhesion coefficient μ have the following relation [18]:

$$F_\mu = \mu \cdot Wg, \tag{5}$$

where Wg is the axle load of the locomotive.

According to (5), a large adhesion coefficient μ equates to a good adhesive force F_μ. Two methods to improve the adhesion coefficient μ are proposed in this study. The first solution is to increase the locomotive axle load. However, the wear between the wheel and the rail also increases due to the pressure of the axle load. The second solution is to fully utilize the current rail surface conditions to obtain the optimal adhesion coefficient $\mu_{\max}$, thereby enhancing the traction power of the locomotive.

The adhesion coefficient μ is not only related to the surface condition of the wheel and rail but also constrained by creep velocity v_s. The following empirical equations are derived based on numerous experimental data and statistical samples [19]:

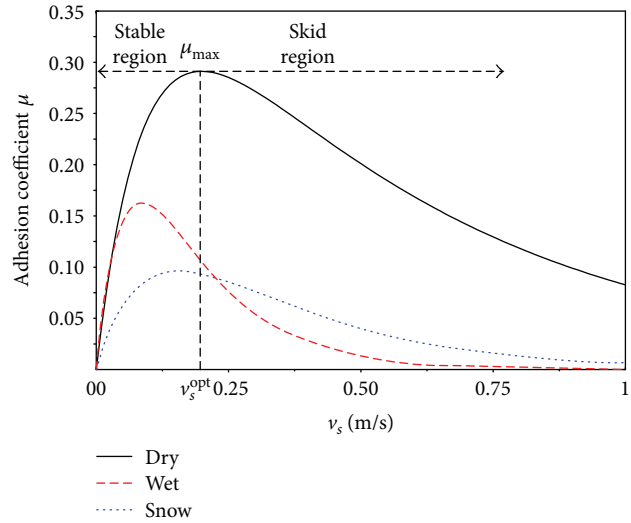

Figure 3: Adhesion characteristic curve.

$$v_s = v_d - v_s,$$
$$\mu = ce^{-av_s} - de^{-bv_s}, \tag{6}$$

where a, b, c, and d are the surface condition coefficients of the wheel and rail, which are positive constants. v_s is the creep speed (m/s).

Figure 3 shows the adhesion characteristic curves under three different wheel-rail surface conditions. Although different optimal adhesion coefficients $\mu_{\max}$ exist in different rail surface conditions, they all exhibit the same trends. That is, the adhesion coefficient increases to $\mu_{\max}$ with the increase of v_s in the stable region and then decreases sharply to zero with the increase of creep v_s after crossing the optimal adhesion point v_s^{opt}. If antiskid measures cannot be immediately obtained, idling or sliding fault becomes inevitable.

According to (3), (4), and (6), the dynamic model of the HHEL is as follows:

$$\begin{bmatrix} \dot{\omega}_m \\ \dot{v}_s \end{bmatrix} = \begin{bmatrix} \dfrac{1}{J_m} \\ \dfrac{r}{J_m R_g^2} \end{bmatrix} T_m + \begin{bmatrix} -\dfrac{1}{J_m} T_L \\ -\dfrac{r^2}{J_m R_g^2} T_L - v_t^2 \end{bmatrix}. \tag{7}$$

Equation (7) shows that the locomotive adhesion control system exhibits strong nonlinear characteristics. The traditional optimal adhesion control method is used to track the given optimal creep velocity v_s^{opt}. This method ensures that the locomotive operates in the optimal adhesion point $\mu_{\max}$ and that the maximal adhesion force is obtained. However, the creep speed v_s fluctuates around the optimal adhesion point v_s^{opt} during the process of tracking. Once the locomotive moves into the skid region, it becomes prone to skidding or idling. Therefore, a control strategy must be established based on the optimal adhesion control to ensure that the creep state is constrained in the stable region.

3. Online Observation of the Wheel-Rail Adhesion Coefficient

In this section, the design step of the adhesion coefficient sliding mode observer is given. First, the traction motor load torque observer is designed to observe the load torque. Then, the wheel-rail adhesion coefficient is further calculated by using the load torque observed value.

3.1. Design of the Sliding Mode Observer. Motor rotor speed ω_m is selected as state variable x_1. Equation (7) is then transformed as follows:

$$\begin{aligned} x_1 &= \omega_m, \\ \dot{x}_1 &= \frac{1}{J_m} T_m - \frac{1}{J_m} T_L. \end{aligned} \tag{8}$$

The sliding mode observer is designed as follows:

$$\begin{aligned} \hat{x}_1 &= \hat{\omega}_m, \\ \dot{\hat{x}}_1 &= \frac{1}{J_m} T_m + \eta_1 \operatorname{sgn}(x_1 - \hat{x}_1), \end{aligned} \tag{9}$$

where $\hat{x}_1$ is the observed value of x_1 and η_1 is a designed gain.

The observer error is defined as follows:

$$e_1 = x_1 - \hat{x}_1. \tag{10}$$

Substituting (9) and (8) into (10) yields

$$\dot{e}_1 = -\frac{1}{J_m} \hat{T}_L - \eta_1 \operatorname{sgn}(e_1). \tag{11}$$

3.2. Online Observation of the Wheel-Rail Adhesion Coefficient. The observation error e_1 is selected as the sliding surface.

$$s_1 = e_1. \tag{12}$$

Theorem 1. *Considering the system (8) and its observer (9), if the sliding surface is set as (12) and if η_1 is sufficiently large enough for any initial $x_0 \in R^n$, e_1 causes global asymptotic convergence to zero.*

Proof. The Lyapunov function is selected as follows:

$$V_1 = \frac{1}{2} s_1^2. \tag{13}$$

Substituting (11) to (13) yields

$$\begin{aligned} \dot{V}_1 = e_1 \dot{e}_1 &= -\frac{e_1}{J_m} T_L - \eta_1 |e_1| \\ &\le |e_1| \left| \frac{1}{J_m} T_L \right| - \eta_1 |e_1| = \left(\left| \frac{1}{J_m} T_L \right| - \eta_1 \right) |e_1|, \end{aligned} \tag{14}$$

where η_1 satisfies $\eta_1 \ge |1/J_m T_L| + \eta_2$ and $\eta_2 > 0$. η_1 and η_2 are constants to be determined.

The following equation is then obtained:

$$\dot{V}_1 \le -\eta_2 |e_1|. \tag{15}$$

According to the Lyapunov stability criterion and sliding mode reaching condition, the error e_1 converges gradually to zero.

This equation completes the proof.

Once the system reaches the sliding surface, (16) can be obtained according to the sliding mode equivalent principle.

$$e_1 = \dot{e}_1 = 0. \tag{16}$$

Substituting (16) into (11), then will yield

$$\hat{T}_L = -J_m \eta_1 \operatorname{sgn}(e_1). \tag{17}$$

The adhesion coefficient can be calculated by substituting (17) into (1) and (5), as shown as follows:

$$\hat{\mu} = \frac{R_g}{rWg} \hat{T}_L. \tag{18}$$

4. Optimal Adhesion Antiskid Control Based on Asymmetric Barrier Lyapunov Function

In this section, firstly, the principle of ABLF is introduced and then, the optimal adhesive antiskid controller is designed and the proof of stability is made.

4.1. ABLF Theory. The following nonlinear system is considered [14]:

$$\begin{aligned} \dot{x} &= f(x) + g(x)u, \\ e &= x - x^*, \end{aligned} \tag{19}$$

where x is the state variable, x^* is a given target, u is the control law, $f(x)$ and $g(x)$ are smooth functions, and e is the error between the actual value x and the given value x^*.

The following BLF is selected [14]:

$$V(e) = \frac{1}{2}\log\frac{k_a^2}{k_a^2 - e^2}. \tag{20}$$

Lemma 1 [15]. *$V(e)$ is continuous and positive definite in an open region $D = \{e \in R : -k_a < e < k_a\}$. $V(e)$ comprises continuous first-order partial derivatives $\dot{V}(e)$ and is negative definite and continuous. If $e \to k_a$ or $e \to -k_a$, $V(e) \to \infty$. A positive constant p exists. When $e(0) < D, \forall\, t \geq 0$, then $e(t) \in D$, $V(e) < p$.*

The schematic of a BLF is shown in Figure 4(a). The boundaries of constraint D are strictly symmetric in relation to the origin.

Remark 1. When the BLF is applied to the antiskid wheel control of the locomotive and the optimal creep velocity v_s^{opt} is considered as a tracking target x^*, two problems should be considered.

(i) Stable region: the entire stable region must be included in the boundary of D to satisfy the initial convergence domain $e(0) \leq D$. Therefore, $k_a \geq v_s^{\text{opt}}$.

(ii) Skid region: the tracking target x^* is the peak point v_s^{opt} of the adhesion characteristic curve, and the creep state should be as close as possible to the peak point. k_a is designed as a small constant.

The two problems contradict each other. To solve the different requirements of the two regions, the ABLF method is proposed for the antiskid constraints of the HHEL. With the help of a switch function $q(e)$, D is divided into two parts, that is, $D_a = \{-k_a < e < 0\}$ and $D_b = \{0 < e < k_b\}$. In the stable and skid regions, k_a, k_b are designed to construct the ABLF and achieve the antiskid constraint. The corresponding ABLF schematic is shown in Figure 4(b).

4.2. Design of the ABLF-Based Antiskid Wheel Controller. The ABLF-based antiskid controller for HHEL is designed as follows.

(1) Choose the state variable $x_2 = v_s$.

$$\begin{aligned} x_2 &= v_s, \\ \dot{x}_2 &= \dot{v}_s. \end{aligned} \tag{21}$$

Substituting (7) into (21) yields

$$\dot{x}_2 = f(x_2)u + g(x_2), \tag{22}$$

where $f(x_2) = r/J_m R_g$, $g(x_2) = -(r^2/J_m R_g^2)F_\mu - \dot{v}_t$, and $u = T_m$.

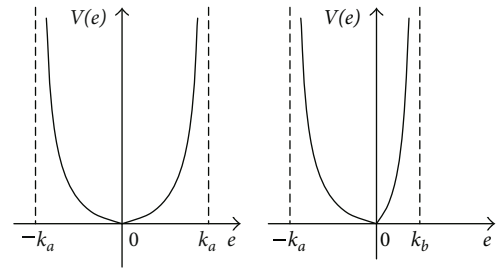

(a) BLF (b) ABLF

Figure 4: BLF schematic.

(2) Define the tracking error e_2.

$$e_2 = x_2 - v_s^*. \tag{23}$$

Substituting (23) into (22) yields the following derivative of error e_2.

$$\dot{e}_2 = f(x_2)u + g(x_2) - \dot{v}_s^*. \tag{24}$$

(3) Design the ABLF as follows:

$$V(e_2) = \frac{1}{2}q(e_2)\log\frac{k_a^2}{k_a^2 - e_2^2} + \frac{1}{2}(1 - q(e_2))\log\frac{k_b^2}{k_b^2 - e_2^2}, \tag{25}$$

where $k_a > v_s^{\text{opt}}$ and $k_b > 0$.

$$q(e_2) = \begin{cases} 1, & \text{as}(e_2 \leq 0), \\ 0, & \text{as}(e_2 > 0). \end{cases} \tag{26}$$

Remark 2. The creep speed tracking error is expressed as e_2, if and only if $e_2 = 0$, in which case $V(e_2) = 0$. If $e_2 \in D$ and $e_2 \neq 0$, $V(e_2) > 0$ and $V(e_2)$ are continuous in $e_2 = 0$. Therefore, $V(e_2)$ is continuous and positive in the open region D.

For the system described by (21) and (22), the control law u is designed as follows:

$$\begin{aligned} u = \frac{1}{f(x_2)}\big(&-g(x_2) + \dot{v}_s^* - q(e_2)k_1 e\big(k_a^2 - e_2^2\big) \\ &- (1 - q(e_2))k_2 e\big(k_b^2 - e_2^2\big)\big), \end{aligned} \tag{27}$$

where $k_1 > 0$ and $k_2 > 0$.

Theorem 2. *For the nonlinear systems described by (23) and (24), if initial error $e_2(0) \in (-k_a, k_b)$, the error is always constrained in the region $D \in (-k_a, k_b)$. Then, variable e_2 gradually converges to zero.*

Proof. The stability proof of the controller is discussed in two cases.

Case 1. When $e_2 \in D$ and $e_2 \le 0$ $q(e_2) = 1$, $V(e_2) = 1/2\log(k_a^2/(k_a^2 - e_2^2))$; its derivative can be obtained as follows:

$$\dot{V}(e_2) = \frac{e_2\dot{e}_2}{k_a^2 - e_2^2} = \frac{e_2}{k_a^2 - e_2^2}\left(f(x_2) + g(x_2)u - \dot{v}_s^*\right). \tag{28}$$

The control law u is changed to u_1.

$$u_1 = \frac{1}{g(x_2)}\left(-f(x_2) + \dot{v}_s^* - k_1 e_2\left(k_a^2 - e_2^2\right)\right). \tag{29}$$

Substituting (31) to (30) yields

$$\dot{V}(e_2) = -k_1 e_2^2. \tag{30}$$

$\dot{V}(e_2) \le 0$ for $D_a = \{e_2 \in R : -k_a < e_2 \le 0\}$ if and only if $e_2 = 0$ and $\dot{V}(e_2) = 0$.

Case 2. When $e_2 \in D$ and $e_2 > 0$ $q(e_2) = 0$, $V(e_2) = 1/2\log(k_b^2/(k_b^2 - e_2^2))$; its derivative can be obtained as follows:

$$\dot{V}(e_2) = \frac{e_2\dot{e}_2}{k_b^2 - e_2^2} = \frac{e_2}{k_b^2 - e_2^2}\left(f(x_2) + g(x_2)u - \dot{v}_s^*\right). \tag{31}$$

The control law u is changed to u_2.

$$u_2 = \frac{1}{g(x_2)}\left(f(x_2) + \dot{v}_s^* - k_2 e_2\left(k_b^2 - e_2^2\right)\right). \tag{32}$$

Substituting (32) to (31) yields

$$\dot{V}(e_2) = -k_2 e_2^2. \tag{33}$$

$\dot{V}(e_2) \le 0$ for $D_b = \{0 < e_2 < k_b\}$, and

$$\lim_{e_2 \to 0^+} \dot{V}(e_2) = \dot{V}(0) = 0. \tag{34}$$

According to (30) and (33), $\dot{V}(e_2)$ is transformed into

$$\dot{V}(e_2) = -q(e_2)k_1 e_2^2 - (1 - q(e_2))k_2 e_2^2. \tag{35}$$

In summary, $V(e_2)$ is a continuous and positive definite scalar function in the open region $D = \{e_2 \in R : -k_a < e < k_b\}$. The derivative of $V(e_2)$ is negative definite and continuous. $\forall\, e_2 \to -k_a$ or $e_2 \to k_b$, $V(e_2) \to \infty$. According to Lemma 1, initial error $e_2(0) \in (-k_a, k_b)$, which is always constrained in the interval $e_2(t) \in (-k_a, k_b)$.

According to the stability proof of the controller in this section, the following is obtained.

(1) $e_2(t) \in (-k_a, k_b)$, $e_2(t)$ is bounded.

(2) $V(0)$, $V(e_2)$ is bounded, and

$$\begin{aligned} V(e_2) &= V(0) + \int_0^t \dot{V}(e_2)dt \\ &= V(0) - \int_0^t \left(q(e_2)k_1 e_2^2 + (1 - q(e_2))k_2 e_2^2\right)dt, \end{aligned} \tag{36}$$

where $\int_0^t (q(e_2)k_1 e_2^2 + (1 - q(e_2))k_2 e_2^2)dt$ is bounded. Obviously, $\int_0^t e_2^2(t)dt$ is bounded.

(3) According to (24),

$$\begin{aligned} \dot{e}_2(t) &= -q(e_2)k_1 e_2\left(\gamma_a^2 - e_2^2\right) \\ &= -(1 - q(e_2))k_2 e_2\left(\gamma_a^2 - e_2^2\right), \end{aligned} \tag{37}$$

where $e_2(t)$ is bounded and $q(e_2)$, k_1, k_2, γ_a, and γ_b are constants. Evidently, $\dot{e}_2(t)$ is bounded.

In summary, variable $e_2(t)$ is bounded; its square integral and derivative are bounded. According to Barbalat's lemma [20], the variable $e_2(t)$ converges gradually.

This equation completes the proof.

Remark 3. According to (23),

$$-k_a + v_s^*(t) < v_s(t) = e_2(t) + v_s^*(t) < k_b + v_s^*(t), \tag{38}$$

where $v_s^*(t) \in (0, v_s^{\text{opt}}]$ and $k_a > v_s^{\text{opt}}$; $\eta_3 = -k_a + v_s^*(t) < 0$ then yields

$$\eta_3 < v_s(t) < k_b + v_s^{\text{opt}}. \tag{39}$$

As shown in the left portion of (37), $\eta_3 < 0$. Considering that the locomotive is running under traction conditions $v_s(t) \ge 0$, then,

$$0 \le v_s(t) < k_b + v_s^{\text{opt}}. \tag{40}$$

The asymmetric constraint target of the creep state can be guaranteed by the design of k_a, k_b. Compared with that of traditional BLF methods, the initial convergence region of the ABLF contains the entire locomotive stable region. The initial convergence condition of the BLF is relaxed.

5. Simulation and Experiment

5.1. Model of the ABLF-Based Antiskid Controller. Figure 5 shows the diagram of the model of the ABLF-based antiskid controller for the HHEL used in the simulation and experiment. The model mainly includes three parts, namely, the locomotive dynamics model, the adhesion coefficient sliding mode observer, and the ABLF controller. The dynamic model of the locomotive is composed of a traction motor control model, a HHEL dynamics model, a locomotive body resistance equation, and an adhesion empirical equation model. The sliding mode observer for the adhesion coefficient estimates the locomotive adhesion coefficient $\hat{\mu}$ with the motor torque signal T_m and motor speed ω_m as input signals. The ABLF control module calculates the control output torque T_m^* with the error between the creep speed v_s and the given optimal creep velocity v_s^{opt}, the adhesion coefficient $\hat{\mu}$, and the differential velocity signal $\dot{v}_t$ of the vehicle body.

Table 1 presents the parameters of the HHEL. The parameters of the optimal creep rate and optimal adhesion coefficient of the three types of rail surfaces are shown in Table 2.

The proposed method is compared with the traditional sliding mode control method to verify the robustness of the

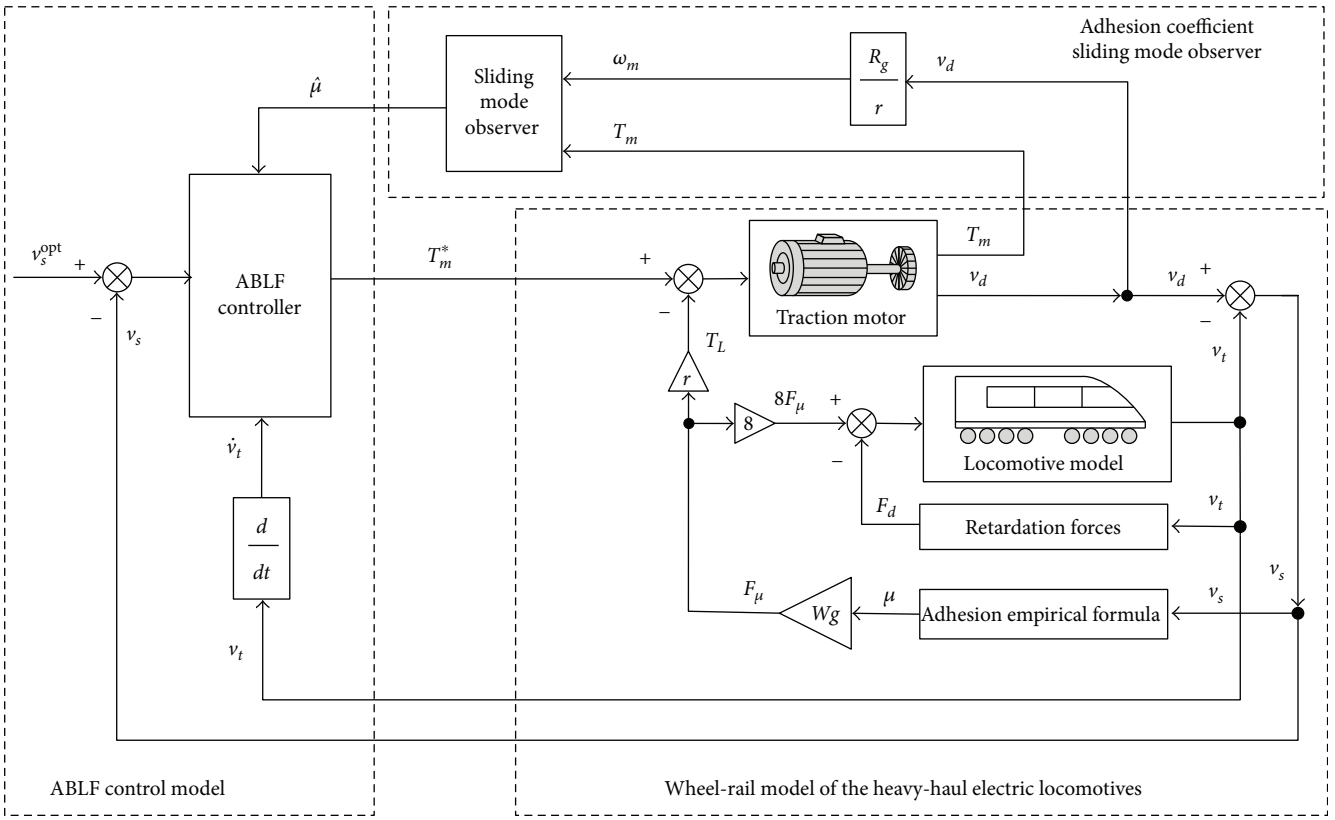

Figure 5: Model of the ABLF-based antiskid controller for HHEL.

Table 1: Parameters of the HHEL.

Parameter	Description	Value
M	Total quality of the locomotive and load	6000 t
W	Single axle load of the locomotive	30 t
J_m	Inertia moment of motor	11 kg·m^2
r	Wheel radius	0.625 m
R_g	Gear speed transfer ratio	6.294

Table 2: Parameters of three types of rail surfaces.

Rail surface	Optimal creep speed	Adhesion coefficient
Dry	0.2 m/s	0.29
Wet	0.085 m/s	0.16
Snow	0.153 m/s	0.06

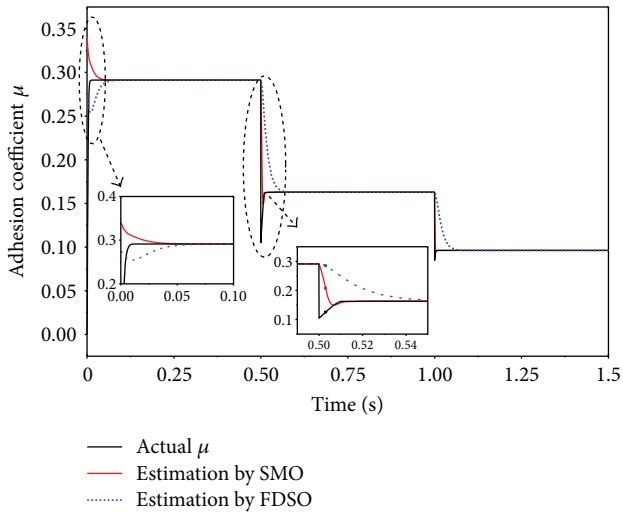

Figure 6: Actual value and observed value by SMO and FDSO of the adhesion coefficient.

ABLF-based control strategy. The rail surface condition gradually deteriorates. At 0–0.5 s, the locomotive starts from the dry rail surface and the optimal creep rate v_s^{opt} is 0.2 m/s. After 0.5 s, the locomotive enters the wet rail and v_s^{opt} changes to 0.085 m/s. After 1 s, the locomotive enters the snow rail and v_s^{opt} becomes 0.153 m/s. The retardation coefficients of the vehicle are $l = 0.5$, $p = 0.041$, and $q = 0.0022$. The ABLF controller gains are $k_1 = 1000$ and $k_2 = 1000$. The barrier boundaries are $k_b = 0.01$ and $k_a = v_s^{opt} + k_b$. The switching gains of the sliding mode controller are $c = 0.1$, $\xi = 10$, and $\lambda = 10$.

5.2. Simulation Results. The simulation results are shown in Figures 6–10. Figure 6 shows the actual value, the estimation

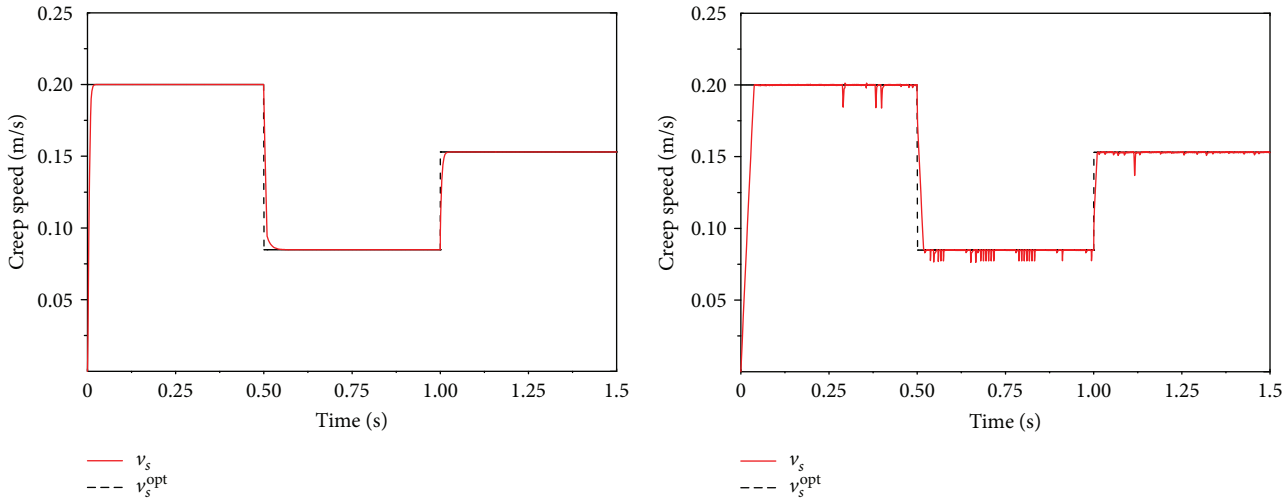

(a) ABLF control (b) SMC control

Figure 7: Given value and actual value of the creep speed.

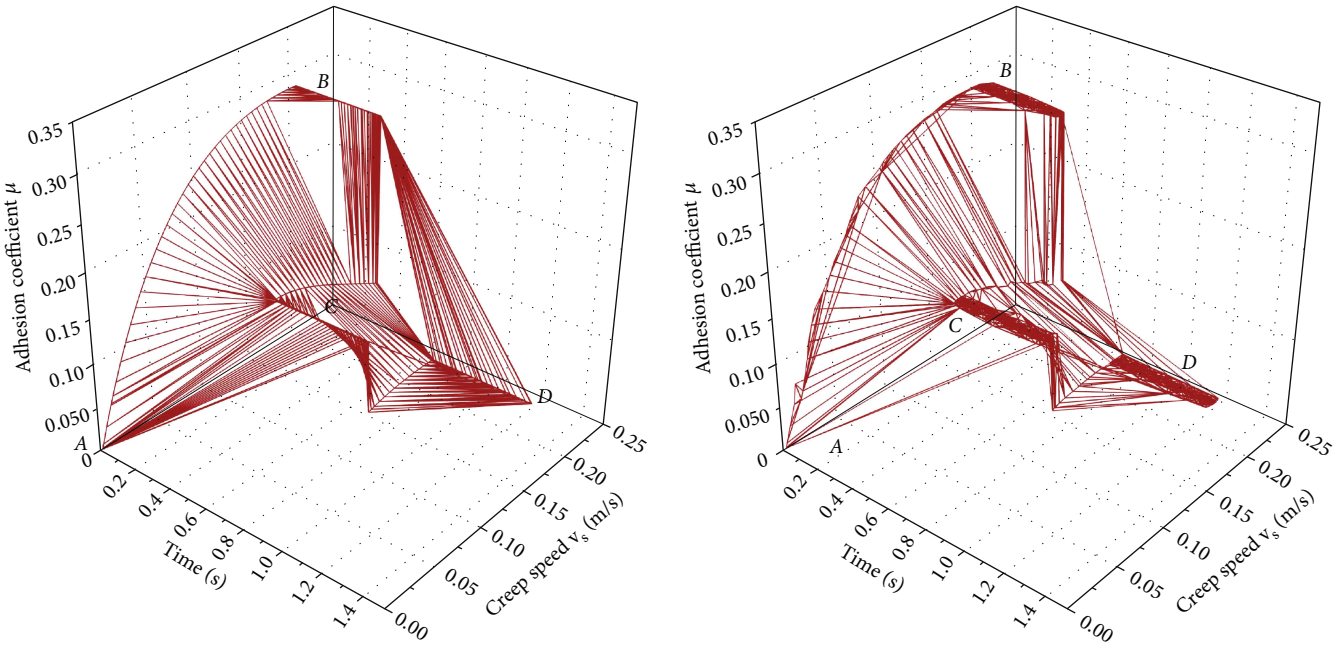

(a) ABLF control (b) SMC control

Figure 8: Adhesion characteristic curve.

by sliding mode observer (SMO), and the estimation by full-dimension state observer (FDSO) [21] of the adhesion coefficient. Firstly, the SMO tracks the actual adhesion value at 0.05 s, and the FDSO tracks the actual adhesion value at 0.07 s. Secondly, when the rail surface switches to the wet surface, the SMO tracks the actual value of the adhesion coefficient at 0.51 s, and the FDSO achieves it at 0.54 s. Finally, the SMO performs better observation effectiveness than the FDSO again, in which the rail surface switches to the snow surface. The sliding mode observer achieves excellent observation effectiveness at the whole stage.

Figure 7 shows the tracking results of the creep speed of the locomotive. Figure 8 shows the adhesion characteristic curve of the creep speed. The locomotive is driven from point *A* in the dry rail. The creep speed is stable at 0.2 m/s and the adhesion coefficient is stable at 0.29. At 0.5 s, the rail surface is changed into the wet rail surface, the adhesion point moved toward the adhesion point *B*, the creep speed is stable at 0.08 m/s, and adhesion coefficient is stable at 0.16. At 1 s, the rail surface is changed into the wet rail surface once again, the creep speed and adhesion coefficient still have good stability. Compared with the traditional sliding mode control technique, the ABLF controller not only converges quickly

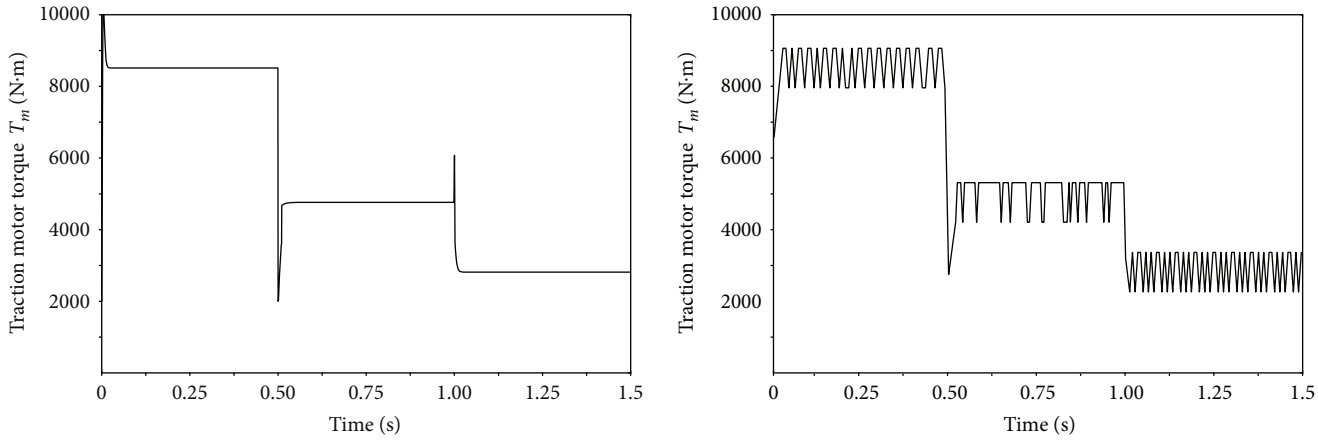

(a) ABLF control

(b) SMC control

Figure 9: Motor output torque.

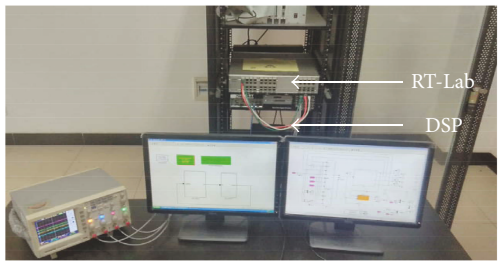

Figure 10: RT-Lab experimental platform.

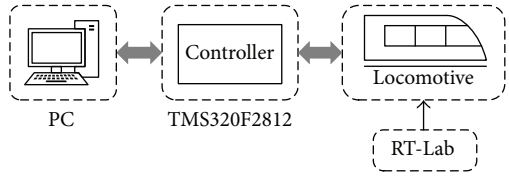

Figure 11: Loop system configuration diagram of RT-Lab.

and minimizes the steady-state error but also avoids the chattering phenomenon of the sliding mode control after reaching the optimal adhesion point.

Figure 9 shows the output torque waveform of the locomotive traction motor. At 0.5 s and 1 s, the output torque T_m of the traction motor changes with the change of the wheel-rail surface condition. The difference between the two methods is that the control torque of the ABFL controller changes only when the rail surface condition switches and that the control torque shows no fluctuation in the steady state. As a result of the chattering of the SMC method, the chattering of the control torque always occurs in the entire process.

5.3. Experimental Results. RT-Lab is a powerful modular real-time simulation platform, which can be used as rapid control prototyping and hardware-in-the-loop simulation (HILS) [22]. Figure 10 shows the RT-Lab experimental platform used in this work. Figure 11 presents the RT-Lab HILS configuration diagram of the ABLF control system of the HHEL. The C program code of the ABLF controller and sliding mode observer is downloaded to the DSP controller TMS320F2812 using a PC. Then, the HHEL model is compiled and downloaded to OP5600, and the HILS of the ABLF control system of the HHEL can be realized. The DSP can use the vehicle speed, wheel speed, motor torque, and optimal value of creep speed as the input signal of the controller. Sampling period is set to 10 μs.

Figure 12 shows the experimental waveforms of the actual and observed values by the SMO and FDSO. The experimental results show that the SMO can accurately track the actual adhesion coefficient, and the performance of the SMO is better than that of the FDSO. Figure 13 shows the experimental values of the given and actual values of creep velocity. The result shows that the ABLF controller can asymptotically track the given value of the creep speed. Figure 14 shows the experimental waveforms of the motor control torque using the two control strategies. The ABLF control strategy clearly shows good control precision in the steady state, thus avoiding the chattering of the traditional sliding mode control method.

6. Conclusions

This paper proposes a new method of online accurate estimation of wheel-rail adhesion coefficient and optimal adhesion antiskid control of heavy-haul electric locomotives (HHEL) based on sliding mode and asymmetric barrier Lyapunov function (ABLF) theory. The following conclusions can be drawn from the results obtained with the proposed method.

(1) A dynamic model of a HHEL was derived, and the adhesion mechanism of the HHEL is analyzed.

(2) The difficulty of measuring adhesion coefficients with a conventional physical sensor is solved, by designing

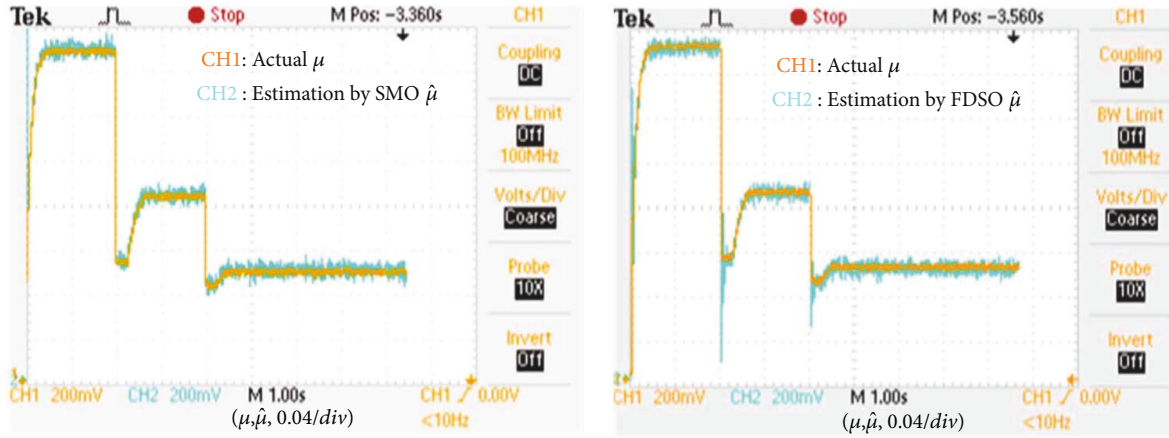

(a) SMO (b) FDSO

Figure 12: Actual value and observed value of the adhesion coefficient by SMO and FDSO.

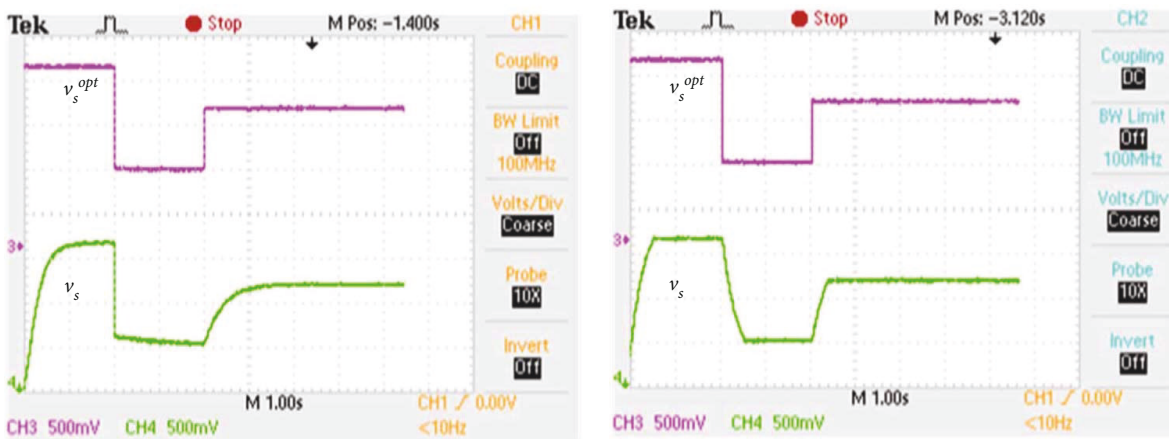

(a) ABLF control (b) SMC control

Figure 13: Given value and actual value of the creep speed.

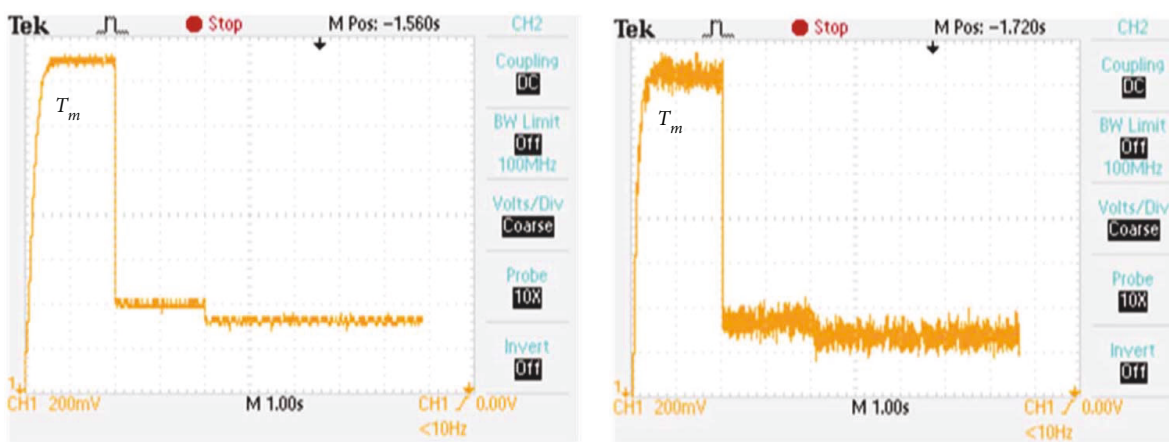

(a) ABLF control (b) SMC control

Figure 14: Motor output torque.

a sliding mode observer which can online accurately observe the adhesion coefficient in real time.

(3) An optimal adhesion antiskid controller is designed based on the ABLF theory. The proposed controller achieved asymmetric control according to the different creep states of the HHEL, which ensures that the creep state is constrained in the stable region. In contrast to existing antiskid control methods, the proposed method reduces the torque ripple of motors. The adhesion control performance of the HHEL is improved.

Conflicts of Interest

The authors declare no conflict of interest.

Authors' Contributions

Kaihui Zhao proposed the ABLF antiskid control scheme and derived the dynamic model of the locomotive. Peng Li and Kaihui Zhao designed the overall algorithms and the simulations. Peng Li, Yanfei Li, and Tonghuan Yin performed the experiments and simulations; Kaihui Zhao and Peng Li wrote the manuscript. Changfan Zhang and Jing He supervised the work and revised the paper.

Acknowledgments

This work is supported by the Natural Science Foundation of China under Grant nos. 61773159, 61473117, and 61733004, the Scientific Research Fund of the Hunan Province Education Department under Grant nos. 16A058 and 17B073, the Natural Science Foundation of China of Hunan Province under Grant nos. 2018JJ2093, 2017JJ4031, and 2016JJ5012, the Hunan Province Education Department under Grant no. 13CY018, the Teaching Reform Fund of Hunan Province Education Department under Grant no. Hunan Education Notice [2016] no. 400, the Teaching Reform of Degree and Postgraduate Education Fund of Hunan University of Technology under Grant no. JG1604, and the Key Laboratory for Electric Drive Control and Intelligent Equipment of Hunan Province Grant no. 2016TP1018.

References

[1] Z. Shi, K. Wang, L. Guo, and Z. Chen, "Effect of arc surfaces friction coefficient on coupler stability in heavy haul locomotives: simulation and experiment," *Vehicle System Dynamics*, vol. 55, no. 9, pp. 1368–1383, 2017.

[2] C. Luna, J. Lázaro, M. Mazo, and A. Cano, "Sensor for high speed, high precision measurement of 2-D positions," *Sensors*, vol. 9, no. 12, pp. 8810–8823, 2009.

[3] L. Wenli, Z. Leiting, and D. Kan, "Performance analysis of re-adhesion optimization control based on full-dimension state observer," *Procedia Engineering*, vol. 23, pp. 531–536, 2011.

[4] P. Pichlík and J. Zděnek, "Extended Kalman filter utilization for a railway traction vehicle slip control," in *2017 International Conference on Optimization of Electrical and Electronic Equipment (OPTIM) & 2017 Intl Aegean Conference on Electrical Machines and Power Electronics (ACEMP)*, pp. 869–874, Brasov, Romania, May 2017.

[5] A. Sabanovic, "Variable structure systems with sliding modes in motion control-a survey," *IEEE Transactions on Industrial Informatics*, vol. 7, no. 2, pp. 212–223, 2011.

[6] C. Zhang, Y. Huang, and R. Shao, "Robust sensor faults detection for induction motor using observer," *Journal of Control Theory and Applications*, vol. 10, no. 4, pp. 528–532, 2012.

[7] C. Zhang, J. Sun, J. He, and L. Liu, "Online estimation of the adhesion coefficient and Its derivative based on the cascading SMC observer," *Journal of Sensors*, vol. 2017, Article ID 8419295, 11 pages, 2017.

[8] Y. Chen, H. Dong, J. Lu, X. Sun, and L. Guo, "A super-twisting-like algorithm and Its application to train operation control with optimal utilization of adhesion force," *IEEE Transactions on Intelligent Transportation Systems*, vol. 17, no. 11, pp. 3035–3044, 2016.

[9] B. Liu, T. X. Mei, and S. Bruni, "Design and optimisation of wheel-rail profiles for adhesion improvement," *Vehicle System Dynamics*, vol. 54, no. 3, pp. 429–444, 2016.

[10] M. Yamashita and T. Soeda, "Anti-slip re-adhesion control method for increasing the tractive force of locomotives through the early detection of wheel slip convergence," in *2015 17th European Conference on Power Electronics and Applications (EPE'15 ECCE-Europe)*, pp. 1–10, Geneva, Switzerland, September 2015.

[11] W. Yang, W. Cai, and Y. Song, "A barrier Lyapunov function (BLF) based approach for antiskid traction/braking control of high speed trains," in *The 26th Chinese Control and Decision Conference (2014 CCDC)*, pp. 5023–5028, Changsha, China, June 2014.

[12] W.-C. Cai, D.-Y. Li, and Y.-D. Song, "A novel approach for active adhesion control of high-speed trains under antiskid constraints," *IEEE Transactions on Intelligent Transportation Systems*, vol. 16, no. 6, pp. 3213–3222, 2015.

[13] K. P. Tee and S. S. Ge, "Control of nonlinear systems with full state constraint using a barrier Lyapunov function," in *Proceedings of the 48h IEEE Conference on Decision and Control (CDC) held jointly with 2009 28th Chinese Control Conference*, pp. 8618–8623, Shanghai, China, December 2009.

[14] K. P. Tee, S. S. Ge, and E. H. Tay, "Barrier Lyapunov functions for the control of output-constrained nonlinear systems," *Automatica*, vol. 45, no. 4, pp. 918–927, 2009.

[15] X. Chen, Z. Dai, H. Lin, and Y. Qiu, "Asymmetric barrier Lyapunov function-based wheel slip control for antilock braking system," *International Journal of Aerospace Engineering*, vol. 2015, Article ID 917807, 10 pages, 2015.

[16] M. Spiryagin, P. Wolfs, C. Cole, and V. Spiryagin, *Design and Simulation of Heavy Haul Locomotives and Trains*, CRC Press, Boca Raton, FL, USA, 2016.

[17] A. Steimel, *Electric Traction-Motive Power and Energy Supply: Basics and Practical Experience*, Oldenbourg Industrieverlag, Munich, Germany, 2008.

[18] Y. Yuan, Z. Hong-Jun, L. Ye-Ming, and L. Shi-Hui, "The dynamic study of locomotives under saturated adhesion," *Vehicle System Dynamics*, vol. 49, no. 8, pp. 1321–1338, 2011.

[19] S. Sadr, D. A. Khaburi, and J. Rodriguez, "Predictive slip control for electrical trains," *IEEE Transactions on Industrial Electronics*, vol. 63, no. 6, pp. 3446–3457, 2016.

[20] J. A. Gallegos, M. A. Duarte-Mermoud, N. Aguila-Camacho, and R. Castro-Linares, "On fractional extensions of Barbalat lemma," *Systems & Control Letters*, vol. 84, pp. 7–12, 2015.

[21] W. L. Lin, Z. G. Liu, and Y. T. Fang, "Re-adhesion optimization control strategy for metro traction," *Journal of Southwest Jiaotong University*, vol. 47, no. 3, pp. 465–470, 2012.

[22] H. Wu, C. Zhang, J. He, and K. Zhao, "Distributed fault-tolerant consensus tracking for networked non-identical motors," *Journal of Industrial and Management Optimization*, vol. 13, no. 2, pp. 917–929, 2017.